NeuroImage 200 (2019) 405–413

Contents lists available at ScienceDirect

NeuroImage

journal homepage: www.elsevier.com/locate/neuroimage

Differential coupling between subcortical calcium and BOLD signals during evoked and resting state through simultaneous calcium fiber photometry and fMRI

Chuanjun Tong [a,b], Jian-kun Dai [b], Yuyan Chen [b], Kaiwei Zhang [b], Yanqiu Feng [a,**], Zhifeng Liang [b,c,*]

[a] School of Biomedical Engineering, Guangdong Provincial Key Laboratory of Medical Image Processing, Key Laboratory of Mental Health of the Ministry of Education, Southern Medical University, Guangzhou, China
[b] Institute of Neuroscience, CAS Center for Excellence in Brain Sciences and Intelligence Technology, Chinese Academy of Sciences, Shanghai, China
[c] Key Laboratory of Primate Neurobiology, Chinese Academy of Sciences, Shanghai, China

A B S T R A C T

Task based and resting state fMRI has been widely utilized to study brain functions. As the foundation of fMRI, the underlying neural basis of the BOLD signal has been extensively studied, but the detailed mechanism remains elusive, particularly during the resting state. To examine the neurovascular coupling, it is important to simultaneously record neural and vascular signals. Here we developed a novel setup of camera based, scalable simultaneous calcium fiber photometry and fMRI in rats. Using this setup, we recorded calcium signals of superior colliculus (SC) and lateral geniculate nucleus (LGN) and fMRI simultaneously during visual stimulation and the resting state. Our results revealed robust, region-specific coupling between calcium and BOLD signals in the task state and weaker, whole brain correlation in the resting state. Interestingly, the spatial specificity of such correlation in the resting state was improved upon regression of white matter, ventricle signals and global signals in fMRI data. Overall, our results suggest differential coupling of calcium and BOLD signals for subcortical regions between evoked and resting states, and the coupling relationship in the resting state was related with resting state BOLD preprocessing strategies.

1. Introduction

Since its advent almost three decades ago, blood oxygenation level-dependent (BOLD) functional magnetic resonance imaging (fMRI) has been widely used for mapping brain activity in the human and animals. The BOLD contrast has been linked to neural activity through the neurovascular coupling process, which is generally believed to arise from the interplay of neural activity, cerebral blood flow (CBF), cerebral blood volume (CBV) and cerebral metabolic rate of oxygen (CMR_{O2}) (Kim and Ogawa, 2012). Extensive research has been conducted to elucidate the detailed mechanism of neurovascular coupling, as it is the physiological foundation for BOLD fMRI. Simultaneous electrophysiological recording and fMRI studies in the macaque cortex showed strong coupling between the BOLD signal and neural responses (as characterized by local field potential and multi-unit activity) during visual stimulation (Goense and Logothetis, 2008; Logothetis et al., 2001). Simultaneous electrophysiological recording and intrinsic optical imaging studies have also in general indicated the similar conclusion (Hillman, 2014).

In addition to the previous neurovascular coupling studies in stimulus evoked states, it has become increasingly important to examine the such relationship during the resting state with the growing applications of resting state fMRI. The current model of the BOLD contrast mechanism relies on the decreased oxygen extraction fraction (OEF) during the period of increased neural activity, and such model might not be able to directly extend to the resting state during which no stimulus evoked neural activation is present. Similar to studies focusing on the stimulus evoked state, simultaneous or sequential electrophysiological recording and fMRI studies in animals have provided some evidence for the neural basis of the resting state BOLD signal and resulting functional connectivity (Jaime et al., 2017; Lu et al., 2007, Lu et al., 2016; Magri et al., 2012; Pan et al., 2013; Scholvinck et al., 2010; Shmuel and Leopold, 2008; Thompson et al., 2013, 2014a, 2014b). In general, those studies have supported the notion that various components of the electrophysiological activity (e.g., infraslow or higher frequency bands) contributed to or were correlated with the spontaneous BOLD signal and the resulting functional connectivity.

* Corresponding author. Institute of Neuroscience, CAS Center for Excellence in Brain Sciences and Intelligence Technology, Chinese Academy of Sciences, Shanghai, China.
** Corresponding author.
E-mail addresses: foree@smu.edu.cn (Y. Feng), zliang@ion.ac.cn (Z. Liang).

https://doi.org/10.1016/j.neuroimage.2019.07.006
Received 26 May 2019; Accepted 2 July 2019
Available online 4 July 2019

Outside the MRI scanner, simultaneous optical imaging of neural (calcium) and hemodynamic signals has also provided important information regarding the relationship between spontaneous neural and hemodynamic signals. Ma et al. and Matsui et al. both reported robust correlation between large scale spontaneous calcium and intrinsic optical imaging signals in mice (Ma et al., 2016; Matsui et al., 2016). Through a similar experimental approach, infra-slow activity of calcium signal was linked to the hemodynamic signal (Mitra et al., 2018). At finer spatial scales, simultaneous electrophysiology and two-photon imaging of blood vessels in mice revealed that spontaneous γ band activity regulates arteriole dilation, which in turn may lead to spontaneous fluctuation of local oxygenation level (Mateo et al., 2017). However, another study (Winder et al., 2017) showed that in awake mice, CBV and local field potential (LFP) was correlated to a much weaker extent during the true rest, compared to those during external stimulation or volitional whisking and body movement. Furthermore, spontaneous hemodynamic fluctuations persisted even when local neural activity was blocked (Winder et al., 2017). Therefore, the exact nature of the resting state BOLD signal remains to be examined.

Recently, simultaneous calcium fiber photometry and fMRI has emerged as a powerful tool to examine the neurovascular coupling (Liang et al., 2017; Schlegel et al., 2018; Schmid et al., 2016; Schulz et al., 2012; Schwalm et al., 2017; Wang et al., 2018). Compared to simultaneous electrophysiological recording in the MRI scanner, fiber photometry is not affected by the inherent electromagnetic interference from MRI. In addition, it has great potentials to reveal cell type specific contributions to task evoked or spontaneous BOLD signals (Schlegel et al., 2018; Schulz et al., 2012; Wang et al., 2018). The above studies also generally reported good agreement between calcium and BOLD signals in sensory and optogenetic stimulation or resting state in the rodent brain.

However, the fiber photometry method in general is not scalable to multiple recording sites (see Table 1 in Schlegel et al., 2018), which limits its applications in exploring neural basis of resting state functional connectivity. Recent advance has enabled simultaneous recording of calcium signals from up to 7 sites using a fiber bundle and camera-based approach (Kim et al., 2016). Therefore, to improve the scalability of simultaneous fiber photometry and fMRI, in the current study we successfully modified and combined it with fMRI in rats. Such setup allowed camera based, dual channel simultaneous calcium fiber photometry and fMRI, and can be conveniently scaled up to more brain regions in the future. Furthermore, in contrast to most previous studies focusing on cortical regions, we specifically examined the neurovascular coupling in subcortical regions of superior colliculus (SC) and lateral geniculate nucleus (LGN), taking advantage of the convenient subcortical access of fiber photometry.

Using this novel setup, our results showed robust and region-specific coupling in both SC and LGN for stimulus-related calcium and BOLD signals, which is in good agreement with previous studies. In contrast, the resting state calcium and BOLD signals in both SC and LGN were much less correlated and the coupling exhibited a global, non-specific patterns. Such spatial correlation between resting state calcium and BOLD signals became progressively more specific upon regression of white matter, ventricle signals and global signals in fMRI data. Overall, the above results suggest differential coupling of calcium and BOLD signals for subcortical regions between evoked and resting states, which would require further examination in the future.

2. Method

2.1. Animals and surgery

Adult male Sprague Dawley rats (300–500g, Shanghai Laboratory Animal Center, Shanghai, China) were used for the current study with food and water *ad libitum*. All procedures were approved by the Institutional Animal Care and Use Committee of Institute of Neuroscience, Chinese Academy of Sciences. Rats were anesthetized with isoflurane (4% for induction and 2% for maintenance) and standard stereotaxic surgery procedures followed. Craniotomies were made above the right superior colliculus (SC) and lateral geniculate nucleus (LGN), and 800–1000 nL AAV virus (rAAV-hSyn-Gcamp6f-WPRE-pA, BrainVTA, China) was injected at each location (SC: 6.3 mm rostral and 0.8 mm lateral to bregma, LGN: 4.7 mm rostral and 4.0 mm lateral to bregma) using an microinjector (Nanoject III, Drummond Scientific Company). An optic fiber (0.2 mm diameter) embedded in a 2.5 mm ceramic ferrule (Thorlabs) was inserted above each injection site. Three ceramic screws were placed in the skull far away from injection sites to further secure the head implants. Dental cement was applied around the screws and ceramic ferrule. The animals were returned to home cage for 4 weeks to allow for recovery and viral GCaMP expression.

2.2. Simultaneous calcium fiber photometry and fMRI setup

The overall optical setup was modified from (Kim et al., 2016), and was summarized in Fig. 1. Similar to Kim et al., a 470 nm LED and a 410 nm LED (Thorlabs, M470F1 and M410F1) were used as excitation sources for the Ca^{2+}-dependent and Ca^{2+}-independent isosbestic measurements, respectively. Two LEDs were respectively filtered with 410-10–nm and 470-10–nm bandpass filters (Thorlabs) and fiber coupled into dichroic cube holders each holding a 425 nm longpass dichroic mirror (DMLP425R, Thorlabs) and a 495 nm longpass dichroic mirror (FF495-Di03, Semrock), and coupled into a 7 m long patch cable through an objective (Olympus RMS20X, 0.4 NA). The patch cable had 2 optical fiber bundled together with two ends towards the animal side (custom made by Thorlabs). Each end of the patch cable was connected with one implanted optical fiber in the animal head, and the emitted light was transmitted back through the same patch cable, filtered with 535 nm bandpass fluorescence emission filter (FF01-535/22–25, Semrock) and finally imaged by a CCD camera (Retiga R1, QImaging).

To enable the concurrent recording of multiple channels per fiber, we used a time-division multiplexing strategy to time-sequentially sample each channel (470 nm and 410 nm) individually. Schematic of the time-division multiplexing strategy was shown in Fig. 1C. Briefly, consecutive camera frames were captured using alternating 470 nm and 410 nm excitation source. Both 470 nm and 410 nm excitation durations were 20 ms and spaced 50 ms apart for 40% duty cycle. Excitation power for both 470 and 410 nm at the tip of the fiber was ~30 μW. Images were acquired at 20 Hz frame rate, thus the individual 470 nm and 410 nm frames were sampled at 10 Hz. The optical acquisition was synchronized with fMRI by TTL triggers from the Bruker scanner.

MRI experiments were conducted on a 9.4T Bruker scanner, with an 86 mm diameter volume coil for transmission and 20 mm diameter single loop surface coil for receiving. Animals were initially anesthetized with 4% isoflurane, and a bolus of 0.05 mg/kg medetomidine was injected i.m. followed by continuous subcutaneous infusion of 0.1 mg/kg/h 10 min afterwards. Isoflurane level was then reduced and kept at 0.5%. Animals' temperature and respiration were monitored, and body temperature was maintained at 36.5 ± 0.5 °C (SA Instruments, Inc, USA).

Anatomical images were acquired using a T2 RARE sequence (matrix size = 256 × 256; FOV = 3.2 × 3.2 cm; slice number = 20; slice thickness = 0.8 mm). Functional gradient-echo EPI images were acquired with the following parameters: repetition time (TR) = 1 s; echo time (TE) = 15 ms; matrix size = 80 × 67; FOV = 3.2 × 2.68 cm; slice number = 20; and slice thickness = 0.8 mm, 600 repetitions. A separate optical fiber (Fig. 1B) coupled with a blue laser was used for delivering external visual stimulation (5 Hz flashing light with 10 s ON and 15 s OFF, resulting a inter stimulus interval (ISI) of 25 s), and the tip of the optical fiber for visual stimulation was placed in front of the rat's left eye. Each simultaneous fiber photometry and fMRI session consisted of 6–8 EPI scans, interleaved by visual stimulation scans and resting state scans. Eight rats were used in this study. In total, 22 and 13 simultaneous fiber photometry and fMRI scans were acquired respectively for SC and LGN under visual stimulation, and 33 and 12 scans for SC and LGN in resting

state, respectively. Among those session, 7 scans recorded calcium signals from both SC and LGN under visual stimulation, and 10 scans in resting state (Fig. S1).

2.3. Histology

Each rat was deeply anesthetized by 3% pentobarbital sodium (40 mg/kg) and then perfused with phosphate-buffered saline (PBS) followed by 4% paraformaldehyde in PBS. The brain was removed and stored in 4% paraformaldehyde for one night and then in 30% sucrose solutions in a refrigerator for 3–5 d. A freezing microtome was used to cut each brain into serially ordered 60 μm thick sections. The brain sections were mounted with DAPI and were used to visualize fluorescence to confirm GCaMP expression and the injection site.

2.4. Data analysis

2.4.1. Preprocessing

The overall flow of simultaneous calcium fiber photometry and fMRI data analysis was illustrated in Fig. S2. fMRI data analysis was performed using custom scripts in MATLAB (MathWorks, Natick, MA) and SPM12 (http://www.fil.ion.ucl.ac.uk/spm/). Raw data preprocessing pipeline consisted of converting Bruker data format to NIFTI format, brain extraction using ITK-SNAP (http://www.itksnap.org/), slice timing correction, realignment, and registration to a template (Valdes-Hernandez et al., 2011) (http://www.idac.tohoku.ac.jp/bir/en/db/rb/101028.html) across rats for group analysis. Regression of covariates for resting state data included three cases: (1) 12 head motion (HM) parameters (6 realignment parameters and their 1st order derivatives); (2) HM, white matter (WM), cerebrospinal fluid (CSF) signals; (3) HM, WM, CSF and global signals (GS). Only head motion parameters were used for visual stimulation data. Resting state data were further band-pass filtered at 0.001–0.1Hz, while task state data were high-pass filtered at 0.001Hz. Both resting state and visual stimulation data were spatial smoothed with a Gaussian Kernel (FWHM = 0.8*0.8*0.8 mm^3). The first fifteen volumes of each EPI scan were discarded prior to data analysis to allow magnetization to reach a steady state.

The task-based fMRI data were then analyzed using SPM12. A simple gamma function with faster onset and peak time was used instead of SPM default hemodynamic response function (HRF) (Fig. S3A), to account for faster HRF in rodents than in human. Standard 1st level general linear model (GLM) was applied with 12 motion parameters as nuisance regressors (Fig. S3B). Significantly activated voxels ($p < 0.001$) around the tip of the optical fiber were used as masks for extracting averaged BOLD time series in both task and resting state scans.

GCaMP6f fluorescence signals at 470 nm and 410 nm were obtained by averaging the pixels inside optical fiber cores (red circles in Fig. 1C) in optical images from the CCD camera. Signal baseline drifts were removed by using the MATLAB function polyfit(). Similar to previous studies (Kim et al., 2016; Ma et al., 2016), the 410 nm control signal was regressed from the 470 nm signal using least-squares regression. The fluorescence change (dF/F) was normalized by subtracting the baseline fluorescence from the fiber fluorescence at each time point and then dividing the value by the baseline fluorescence. The calcium and BOLD time series were respectively down-sampled and up-sampled to 5 Hz by using the MATLAB function interp1() and then used for the subsequent HRF estimation.

2.4.2. HRF estimation

To examine the transfer function from calcium to BOLD signals (thereafter we loosely use the term of HRF for convenience), the least-square deconvolution technique was applied (Pedregosa et al., 2015; Rangaprakash et al., 2018). For a linear time-invariant system, the convolution can be expressed as:

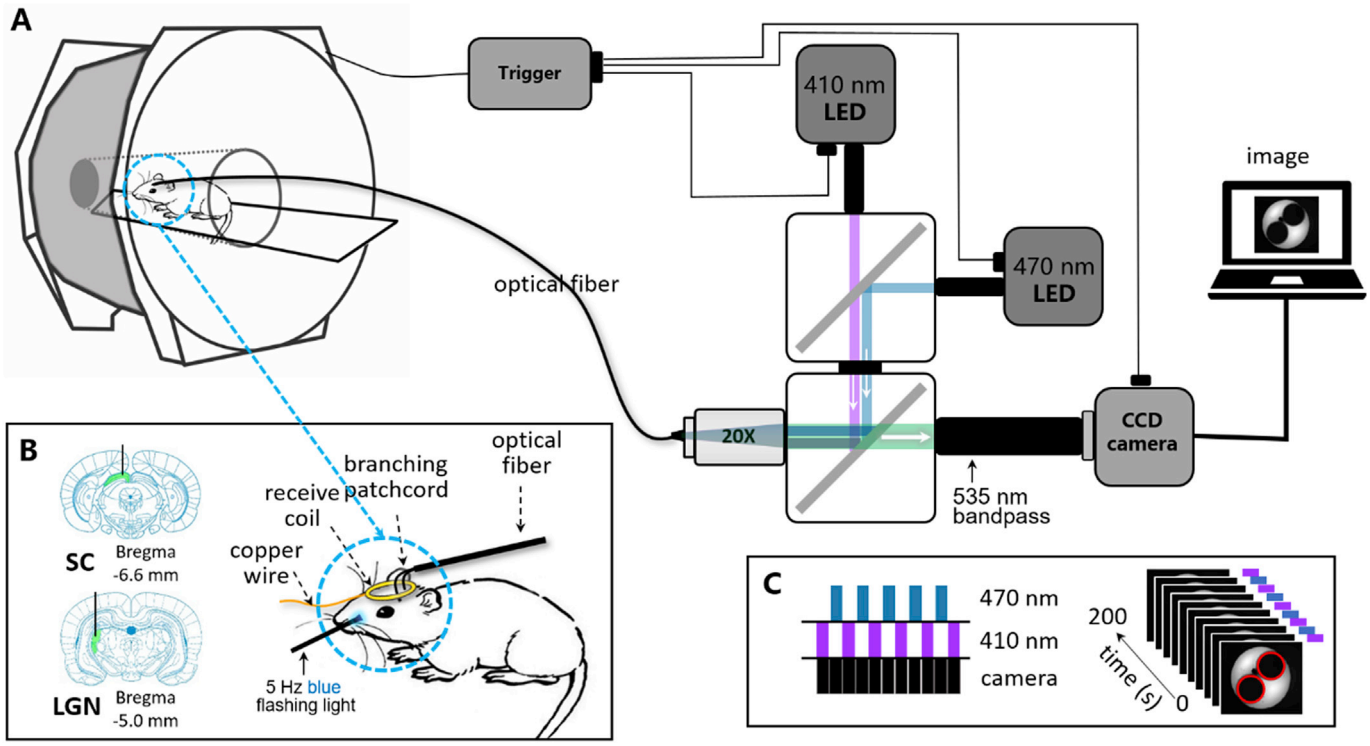

Fig. 1. Schematic illustration of the simultaneous calcium fiber photometry and fMRI setup. (A) upper right, the optical components mounted on an optical table. The optical acquisition was synchronized with fMRI by TTL triggers from the Bruker scanner. Upper left, the anesthetized rat in the scanner bore tethered to the optical patch cable. (B) The fiber-optic implant in the animal head. The green areas were SC and LGN. (C) Left side, the diagram of sequential acquisition of 470 nm and 410 nm channel signals (blue: 470 nm; cyan: 410 nm; black: camera frames). Right side, calcium fiber photometry data from 0 s to 200 s in one scan. The red circles were masks for extracting the optical signals.

$$\begin{bmatrix} y_1 \\ y_2 \\ y_3 \\ \vdots \\ y_n \end{bmatrix} = \begin{bmatrix} x_1 & 0 & 0 & \cdots & 0 \\ x_2 & x_1 & 0 & \cdots & 0 \\ x_3 & x_2 & x_1 & \cdots & 0 \\ \vdots & \vdots & \vdots & \ddots & \vdots \\ x_n & x_{n-1} & x_{n-2} & \cdots & x_{n-m} \end{bmatrix} \begin{bmatrix} 0 & \cdots & 0 \\ 0 & \cdots & 0 \\ x_1 & \cdots & 0 \\ \vdots & \ddots & \vdots \\ x_{n-2} & \cdots & x_{n-m} \end{bmatrix} \cdot \begin{bmatrix} h_1 \\ h_2 \\ h_3 \\ \vdots \\ h_m \end{bmatrix} + \begin{bmatrix} \eta_1 \\ \eta_2 \\ \eta_3 \\ \vdots \\ \eta_n \end{bmatrix}$$

or $\boldsymbol{y} = \boldsymbol{Xh} + \boldsymbol{\eta}$, where $\boldsymbol{X}$ is the system input, which is change in calcium signal; $\boldsymbol{y}$ is the system output, which is BOLD signal; $\boldsymbol{h}$ is the response function, which is the HRF in the context of neurovascular coupling; and $\boldsymbol{\eta}$ is the noise component. As Least Square Errors (LSE) based direct deconvolution amplifies the noise component in the results, we defined a new cost function as follows:

$$\boldsymbol{E}(\hat{\boldsymbol{h}}) = \boldsymbol{y} - \boldsymbol{X}\hat{\boldsymbol{h}}_2^2 + \lambda \nabla_2 \hat{\boldsymbol{h}}_2^2$$

where $\hat{\boldsymbol{h}}$ is the fitting result, the definition of λ is based on 'l-curve' principle (Hansen, 2000) and ∇_2 is 2-order differential operator:

$$\nabla_2 = \begin{bmatrix} 2 & 0 & 0 & \ldots & 0 \\ -1 & -1 & 0 & \ldots & 0 \\ 0 & 2 & -1 & \ldots & \ldots 0 \\ 0 & -1 & 2 & \ldots & 0 \\ \vdots & \vdots & \vdots & \ddots & \vdots \\ 0 & 0 & 0 & \cdots & 2 \end{bmatrix}_{m \times m}$$

MATLAB function lsqnonlin() with lower and upper bounds of $[0\,0 \cdots 0]^{\mathrm{T}}_{m\times 1}$ and $[1\,1 \cdots 1]^{\mathrm{T}}_{m\times 1}$ was then utilized to find the optimal $\hat{\boldsymbol{h}}$, which minimized the cost function of $\boldsymbol{E}$.

2.4.3. Processing

For **N pairs** calcium (corrected fluorescence signal) and BOLD signals (whole brain BOLD time courses), "leave one out" approach was applied to estimate the correlation between calcium and BOLD signals. Firstly, **N-1 pairs** calcium and BOLD signals (extracted from the 4 significantly activated voxels underneath the fiber tip, Fig. S3B) were used for HRF estimations by deconvolution with "ten-folder cross validation". Secondly, the optimal HRF was convolved with the **"remaining one"** calcium signal to generate the predicted BOLD signal. Thirdly, we obtained **one correlation map** between the HRF predicted BOLD and whole brain BOLD time courses (**"remaining one"** BOLD signals). Finally, for **N pairs** calcium and BOLD signals, one sample *t*-test was applied to **N correlation maps** (after Fisher-z transformation) for each voxel. The resulting t-map represented the statistical significance of correlation between calcium predicted time courses and the actual BOLD signals, and the significance level was set to uncorrected $p < 0.005$. Additionally, as a control, time reversed calcium signals were used for the same correlation analysis for the resting state data, similarly with a previous study (Pan et al., 2013).

To probe the correlation between stimulus-related and non-stimulus-related calcium signals and BOLD signals, the calcium signal under visual stimulation was further divided into two components: stimulus-related component (0–0.8 Hz) and non-stimulus-related component (0.8–5 Hz) using a 10-order Butterworth filter. The frequency of the stimulation paradigm was 0.04 Hz (1/25s), therefore the cutoff frequency of 0.8 Hz was chosen to minimize higher harmonics aliasing of the stimulation paradigm frequency.

3. Results

3.1. Novel camera based, dual site simultaneous calcium fiber photometry and fMRI

We established the camera based, dual site simultaneous calcium fiber photometry and fMRI setup (Figs. 1 and 2). Such scalable setup allows dual sites, potentially multiple sites in the future, calcium fiber photometry with additional 410 nm channel as an isosbestic control. Using this setup, evoked calcium signal responses at 470 nm were robustly observed upon visual stimulation (Fig. 2B upper panel and Fig. 2C), while calcium signals with sparse spontaneous firings in resting state were shown in Fig. 2B (lower panel). In addition, small but visible stimulus evoked signal decrease was observed in 410 nm channel (Fig. 2B, upper middle panel). Such decrease might be related to robust hemodynamic changes (e.g., CBV increase) in brain tissues around the optical fiber upon stimulation, which changed the signal intensity at 410 nm channel (Ma et al., 2016). Therefore, such change in the GCaMP isosbestic control signal necessitated the correction of GCaMP 470 nm signals. Regression of 410 nm signals from 470 nm signals clearly altered the temporal pattern in 470 nm signal (Fig. 2C), with more sustained peaks during stimulation and no negative response immediately after the stimulation. Similar results after isosbestic control correction were shown in Fig. S4 for LGN in both task and resting state using the same approach. The expression and location of GCaMP6f protein were verified by histology in all animals (Fig. 2A, left panel).

3.2. Spatiotemporal coupling between calcium and BOLD signals

During visual stimulation, the stimulation paradigm, calcium signal and BOLD signal were clearly correlated with each other for both SC and LGN (Fig. 3A and B, upper panel). An HRF based approach (Fig. S2, see Methods section for details) was utilized to examine the coupling relationship between calcium and BOLD signals. The optimal HRF (Fig. 3E) was deconvolved from pairs of calcium and BOLD signals by "ten-folder cross-validation" approach for both evoked and resting states. Notably the HRFs during visual stimulation were much faster than those during the resting state (time to peak ~2 s v.s. time to peak ~4 s). Calcium signals were then convolved with derived HRFs to generate calcium predicted BOLD signals. Such predicted signals in both SC and LGN showed robust coupling with BOLD signals in visually responsive areas including SC, LGN and part of visual cortex (Fig. 3A and B, middle and lower panels). In contrast, during the resting state, such correlation was much weaker (Fig. 3C and D). Both SC and LGN calcium predicted signals exhibited widespread and non-specific correlation with whole brain BOLD signals, with relative strong correlation in areas immediately under the optical fibers. Importantly, such correlation was not mere noise correlation, as time reversed calcium signals were used as a control, and predicted BOLD signals from those control signals showed almost no correlation at all with the actual BOLD signals (Fig. 3C and D, lower right panels).

To further examine the roles of stimulus-related and non-stimulus-related components in the visual stimulation data, the calcium signals were further divided into two frequency bands (0–0.8 Hz, stimulus-related; 0.8–5 Hz, non-stimulus-related) as described in Methods section, and their HRFs and the relationship with BOLD signals were calculated respectively (Fig. 4 and Fig. S5). It was clear that for the stimulus-related component, the HRFs were similar to those from the broadband calcium data in Fig. 3. Spatially, the stimulus-related spatial correlation between calcium predicted BOLD signal and empirical BOLD signals was robust and region-specific (Fig. 4C, upper panel), which was also similar to those from the broadband stimulation data. For the non-stimulus-related component, the pattern was similar to those from the resting state data (Fig. 4C, lower panels). Spatial correlation maps without thresholding were also shown in Fig. 4D for better visualization of the spatial extent. Similar results were found with LGN calcium recordings (Fig. S5).

We next explored the impact of nuisance signal regression on calcium and BOLD coupling in the resting state. We compared the results from 2 additional resting-state fMRI preprocessing regressor choices: (1) head motion, WM and CSF signals, (2) head motion, WM, CSF and global signals (Fig. 5 and Fig. S6), in addition to the previous head motion only regression shown in Fig. 3. With additional WM, CSF and global signal

regression, the spatial extents of the correlation became gradually reduced (Fig. 5C and Fig. S6C; middle and lower panels). Notably, upon additional global signal regression, only the area immediately under the fiber tip showed significant correlation (Fig. 5C and Fig. S6C; lower panel). Such reduction of spatial correlation among three regressor choices was also mirrored in resting state fMRI based functional connectivity maps (Fig. S7). The above results suggested that potentially different signal components were retained in resting state fMRI data using different preprocessing strategies.

Finally, to take advantage of our dual site fiber photometry recording, we examined whether the strength of dual site calcium signal correlation was correlated with the strength of BOLD signal correlation between SC and LGN. A significant correspondence of calcium and BOLD functional connectivity between SC and LGN was shown in Fig. 6 in both task ($R^2 = 0.82$, $p < 0.01$) and resting states ($R^2 = 0.55$, $p < 0.05$). BOLD functional connectivity between SC and LGN was calculated using resting state fMRI data with head motion only preprocessing. This result provided preliminary evidence of the neural basis of the functional connectivity.

4. Discussion

In the current study, we established a novel scalable, dual site, simultaneous fiber photometry and fMRI setup in rats, and utilized this setup to examine the coupling between the calcium and the BOLD signals in subcortical regions of SC and LGN. Our results suggested differential coupling relationship between calcium and BOLD signals in the task evoked and resting states. Robust and region-specific coupling under visual stimulation was observed while such coupling in the resting state was weaker and non-region-specific. The spatial specificity of such correlation in the resting state was improved upon regression of white matter, ventricle and global signals in fMRI data, suggesting the importance of preprocessing strategies.

4.1. Technical novelty of the simultaneous fiber photometry and fMRI setup

In recent years, simultaneous fiber photometry and fMRI has become a popular technique to acquire neural signals inside the MRI scanner, primarily for its simplicity compared to simultaneous electrophysiology and fMRI (for a detailed comparison between the two techniques, see Table 1 in Schlegel et al., 2018). However, previous studies mostly employed the photon detector based single site recording setup, which cannot be scaled up conveniently or inexpensively to record multiple sites. Camera based fiber photometry has provided a scalable alternative approach for measuring multiple brain regions (up to 8 sites) with comparable performance to the traditional approach (Kim et al., 2016). Therefore, we adopted this approach and combined it with fMRI in rats. Our results clearly demonstrated the feasibility of using this approach inside the scanner, and measuring neural activities from multiple sites simultaneously with fMRI is particularly beneficial for future investigation of neural basis of the functional connectivity, such as the preliminary examination in the current study (Fig. 6).

Another important advantage of the current setup is an additional isosbestic control (410 nm) channel for 470 nm calcium signal. In addition to account for confounding factors like head motion, it has been shown that at the calcium signal acquired by wide field optical imaging was affected by hemodynamic signal changes, as both excitation and emission wavelengths of GCaMP fluorescence can be absorbed by hemoglobin and deoxyhemoglobin (Ma et al., 2016). Our isosbestic control signal clearly showed such interference, when 410 nm channel signal showed stimulus evoked decrease (Fig. 2B, C and Fig. S4A). This decrease is likely due to the CBV increase during visual stimulation. Therefore, acquisition of the 410 nm isosbestic control could reduce the crosstalk of the calcium and hemodynamic signals, which is particularly important for studies examining the coupling of the calcium and BOLD signals.

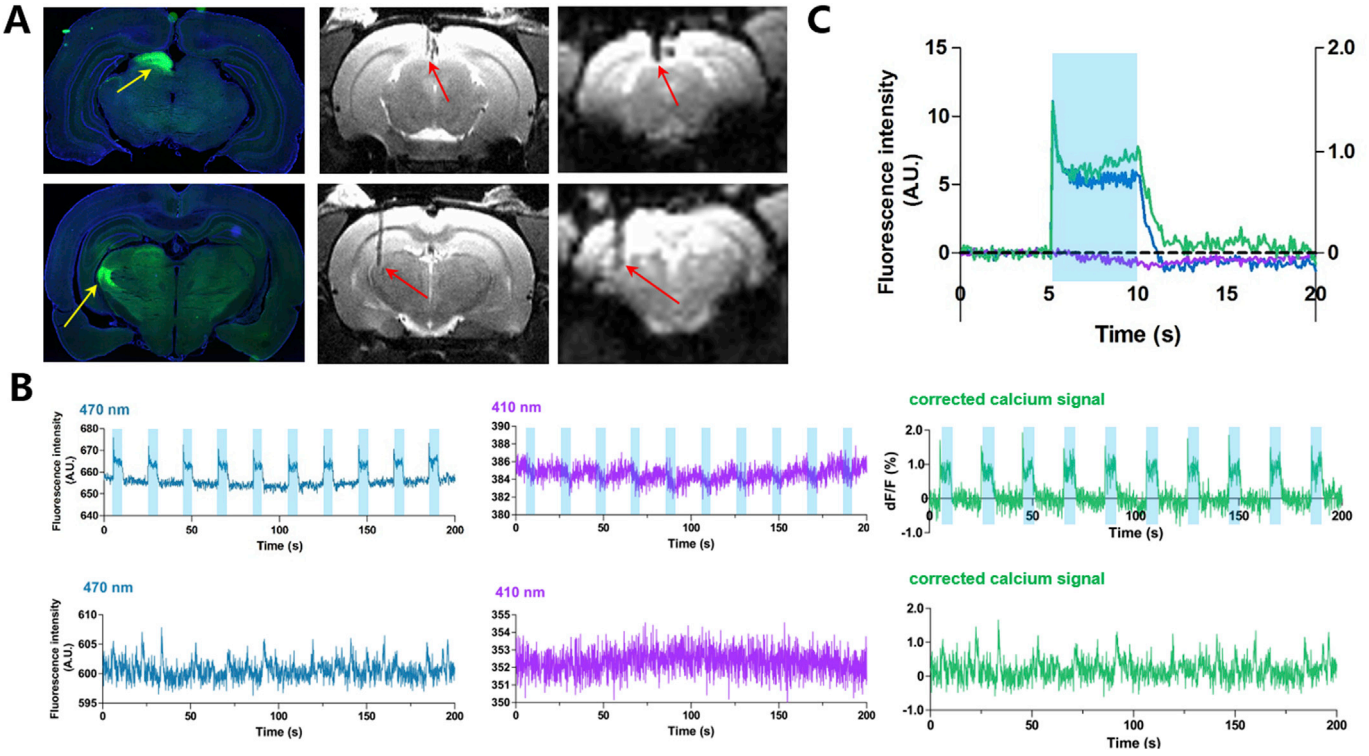

Fig. 2. Stimulus evoked and resting state GCaMP based fiber photometry recording. (A) left panels, histological characterization of GCaMP6f protein expression. Yellow arrows indicated SC and LGN. Middle panels, T2 weighted structural images. Right panels, T2* weighted functional images. Red arrows indicated implanted optical fibers. (B) Stimulus-evoked signals (upper) and resting state signals (lower) in 470 nm and 410 nm channels and the corrected calcium signal by regressing the 410 nm signal from the 470 nm signal in SC. (C) Averaged 470 nm, 410 nm and corrected calcium signals. Blue shades indicated the visual stimulation period.

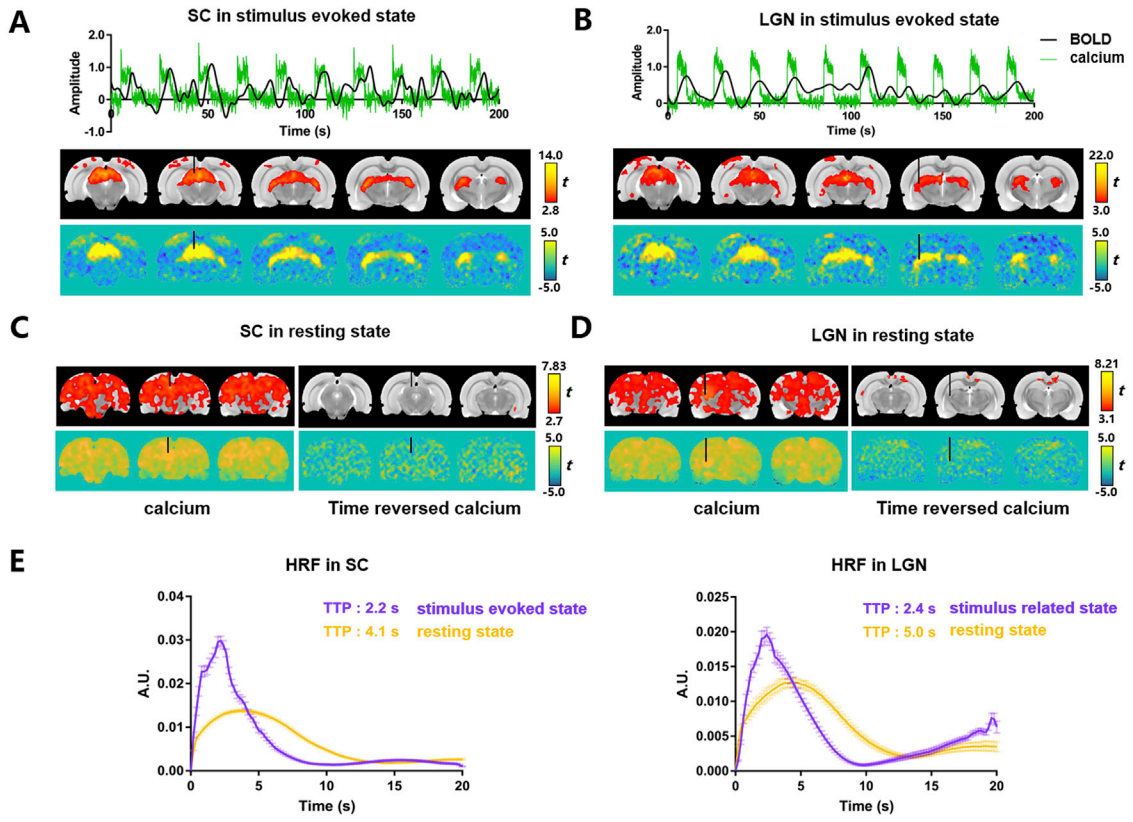

Fig. 3. Correlation between calcium and BOLD signals in SC and LGN in stimulus evoked and resting states. (A, B) Upper panels, representative calcium (green) and BOLD (black) time courses in SC and LGN under visual stimulation. Middle panels, the spatial correlation maps between calcium predicted and empirical BOLD signals (uncorrected $p < 0.005$ with a minimum cluster size of 10 voxels). Lower panels, correlation maps without thresholding. (C, D) Upper panels, the spatial correlation maps between calcium predicted (left) or time-reversed calcium predicted (right) and whole brain BOLD signals (uncorrected $p < 0.005$ with a minimum cluster size of 10 voxels). Lower panels, correlation maps without thresholding. (E) HRFs estimated from evoked and resting state data in SC and LGN. TTP, time to peak.

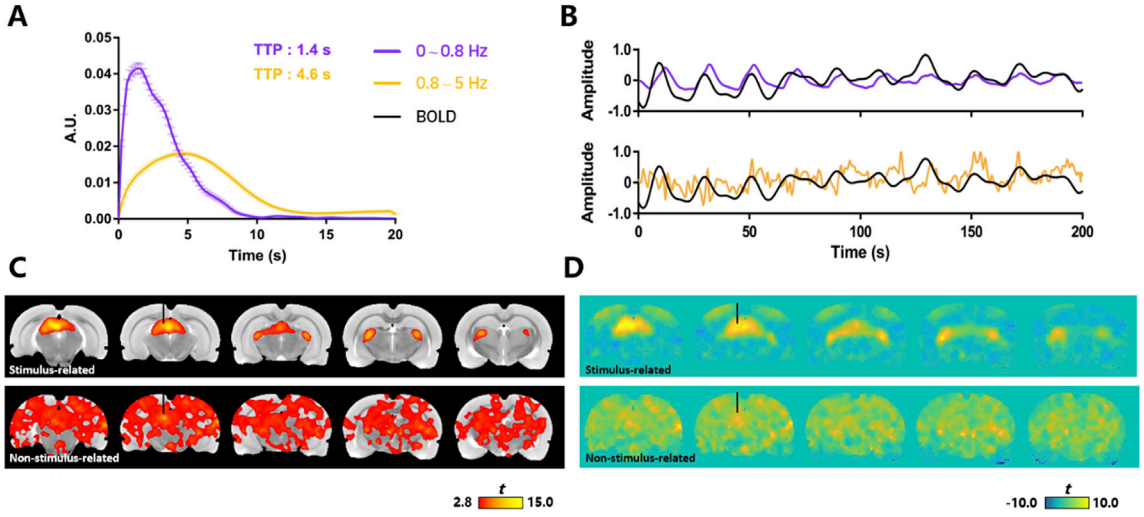

Fig. 4. Stimulus related and non-stimulus-related spatiotemporal coupling between calcium and BOLD signals in SC in the stimulus evoked state. (A) Estimated HRFs based on two frequency bands (stimulus related: 0–0.8 Hz, non-stimulus-related: 0.8–5 Hz) of calcium signals and the simultaneously acquired BOLD signal. (B) Representative time courses of empirical BOLD signals and calcium predicted BOLD signals at two calcium frequency bands (upper, 0–0.8 Hz, lower, 0.8–5 Hz). (C) Spatial correlation maps from two calcium frequency bands (upper, 0–0.8 Hz, lower 0.8–5 Hz). Uncorrected $p < 0.005$ with a minimum cluster size of 10 voxels. (D) Correlation maps without thresholding.

4.2. Validity of subcortical calcium signals in the resting state

It can be clearly noted that the resting state fluctuations of calcium signals from SC and LGN were less prominent compared to the evoked states, and the correlation maps between calcium and BOLD signals were weaker and non-specific, compared to those from the evoked states. It might not be clear whether such results represented biologically relevant features of those two regions or system noises. However, it was less likely

to be the latter case with the argument below:

Firstly, the resting state and visual stimulation sessions were acquired in an interleaved fashion (i.e., for a given animal, a visual stimulation session was acquired, and then followed by a resting state scan and so on). The animal condition and other factors affecting the signals could be assumed almost identical between the task evoked and resting state sessions. Both stimulation evoked calcium signals and BOLD fMRI signals showed good responses to flashing light, suggesting good signal quality. It would be difficult to postulate, under the identical condition, the resting state data were entirely noises. In fact, examples of resting state calcium time series of SC (Fig. 2B) and LGN (Fig. S4B) showed visible spike-like features in the 470 nm channel.

Secondly, our setup included a 410 nm isosbestic control, which was intentionally added in the design to remove potential non-neural fluctuations. We did not observe any significant fluctuations in the 410 nm channel due to non-neural sources (e.g., head motion or hemodynamic artifacts). Even if there were such confounding effects, they would be greatly reduced by regressing out the 410 nm channel signal from the 470 nm channel.

Thirdly, the resting state spatial correlation maps in left panels of Fig. 3C and D (and later Figures) were statistically significant, with the strongest correlation at the tip of the optical fiber. Such patterns suggest the non-random feature of the correlation. In addition, those correlation maps might look like "noisy" due to their global patterns, but such pattern has also been reported before between locally recorded electrophysiological signals and resting state BOLD signals (Fig. 3 in Schölvinck et al., 2010). Importantly, as control analysis, correlations were also calculated between time reversed resting state calcium signals generated BOLD signals and BOLD time series (Fig. 3C and D; right panels). Such "time reversed" control has been applied to coherence analysis between LFP and BOLD signals in a previous study (Pan et al., 2013). Those control t-maps showed almost no correlation at all, which was very different from the correlation maps from the actual resting state calcium signals. This sharp contrast also suggests the observed patterns were less likely to arise from pure noises. Moreover, the spatial specificity of such correlation was much improved when more nuisance regressors were applied (Fig. 5 and Fig. S6), further suggesting its potential biological relevance.

Fourthly, as primary sensory relay nucleus, it is not surprising that both SC and LGN exhibit lower baseline firing rates, compared to stimulation periods. For example, our previous study showed SC baseline firing rate was much lower compared to the stimulus evoked condition (Fig. 3A, Liang et al., 2017). Even during the same resting state, subcortical primary sensory nuclei generally show lower firing rates compared to the cortex. This might in part contribute to the discrepancy between the current subcortical recordings and previous cortical, especially S1, recordings in earlier studies (Schlegel et al., 2018; Schwalm et al., 2017). Overall, it was not unreasonable to observe less prominent fluctuations in the subcortical resting state calcium signals.

Taken together with the points discussed above, it is likely that the reported results here were not entirely due to noises. However, it might still be possible that actual signal in the resting state was so weak that the recorded signal was dominated by system noises. Even in such "worst case scenario", we argue that the current data could provide valuable information to the field: the resting state calcium signals in SC and LGN were much weaker than the evoked state. This will require caution when interpreting resting state BOLD fMRI results from such subcortical regions.

4.3. Differential neurovascular coupling in task and resting state

In our present study, during the visual stimulation calcium signals from both SC and LGN, two visually responsive subcortical regions, were robustly coupled with the BOLD responses (Figs. 3 and 4 and Fig. S5). Not surprisingly, further examination showed such coupling was mainly contributed by the stimulus-related component (0–0.8 Hz) which included the basis frequency of the task paradigm (0.04 Hz), both in terms of temporal characteristics (i.e., HRF shapes) and spatial correlation patterns (Fig. 4 and Fig. S5). In contrast, at non-stimulus-related frequency band (0.8–5 Hz) temporal and spatial coupling patterns were similar to these the resting state data. Therefore, it can be speculated that the coupling in the stimulus evoked state can be divided into two components: stimulus related, fast and spatially specific one and non-stimulus-related, resting state like, weaker and non-region-specific one.

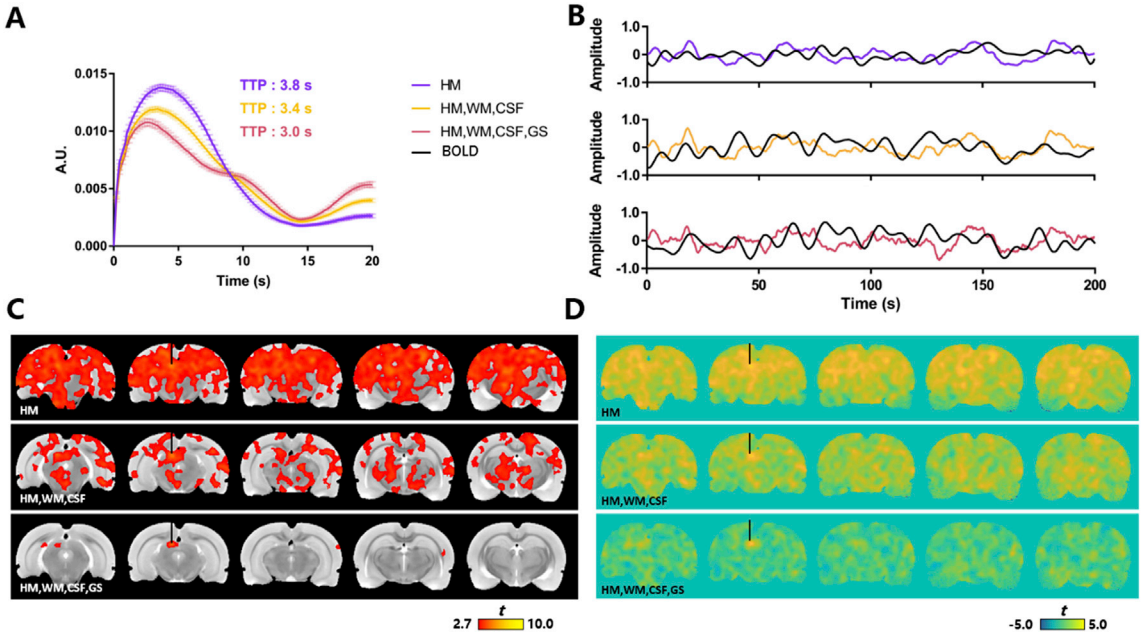

Fig. 5. Impact of three nuisance regressor choices in SC on the resting state coupling between calcium and BOLD signals. (A) Estimated HRFs based on the calcium signal and the simultaneously acquired BOLD signal with three nuisance regressor choices. (B) Representative time courses of calcium predicted BOLD signals and empirical BOLD signals with three nuisance regressor choices. (C) Spatial correlation maps with uncorrected $p < 0.005$ and a minimum cluster size of 10 voxels. (D) Correlation maps without thresholding. HM, head motion. WM, white matter. CSF, cerebrospinal fluid. GS, global signal.

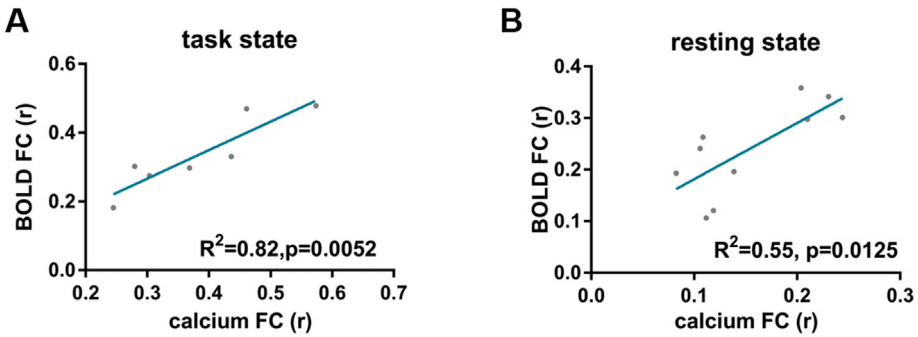

Fig. 6. The correspondence of calcium and BOLD functional connectivity (FC) between SC and LGN in task (A) and resting states (B). The correspondence of calcium and BOLD FC was generated from dual site (SC and LGN) calcium and BOLD recordings. The calcium (or BOLD) FC was the Pearson correlation coefficient between the calcium (or BOLD) signal of SC and the calcium (or BOLD) signal of LGN.

Such notion of separable evoked and spontaneous activities in the evoked state has long been previously proposed (Fox et al., 2006) and the current study might further support such notion from a neurovascular coupling perspective.

It was surprising, but not entirely unexpected, to observe the whole brain, non-specific correlation patterns in the resting state in both SC and LGN. Both Schwalm et al. and Schlegel et al. reported cortex wide correlation from a locally recorded cortical calcium signal (Schlegel et al., 2018; Schwalm et al., 2017), but it is unclear whether those studies performed any regression (e.g., motion parameters, white matter, ventricle or global signals) on their resting state fMRI. Another earlier study, using electrophysiology and fMRI in macaques, also reported widespread correlation in resting state fMRI from locally recorded LFP signals (Scholvinck et al., 2010). The above studies all focused on the cortical regions, and the current study provided additional evidence of such whole brain correlation from subcortical recordings in the resting state.

Interestingly, such spatial coupling in the resting state was dependent on the preprocessing strategies of fMRI data. Upon additional regression of white matter, ventricle and global signals, the global correlation was drastically reduced to a small area under the tip of the optical fiber. Regression of white matter/ventricle and/or global signals is common in resting state fMRI preprocessing, which is generally believed to remove unwanted residual motion and non-neural physiological fluctuations in the resting state data, although the use of global signal regression is not without controversy. The drastic effect of the additional nuisance regression resembled the known effect of such regression on resting state functional connectivity (Fox et al., 2009), which was also observed in our data (Fig. S7). Therefore, we speculate that in the resting state, the neural activities and related coupling can also be divided into whole brain and local components. It would further suggest that in the resting state fMRI preprocessing, both minimal (i.e., head motion only) and full nuisance regression might both reflect potentially different parts of underlying neural fluctuations, and the choice of the regression will ultimately depend on the specific research questions.

In addition to the temporal and spatial differences to the evoked activity related coupling, one noticeable difference in the non-evoked activity related coupling was its much weaker coupling strength. Such weaker correlation was in great agreement with a recent simultaneous optical imaging and electrophysiology study in awake mice (Winder et al., 2017), but in contrary to other studies (Ma et al., 2016; Mateo et al., 2017; Matsui et al., 2016; Schlegel et al., 2018; Schwalm et al., 2017). Winder et al. reported a strong coupling between local field potential and CBV signals in the somatosensory cortex during whisker stimulation and volitional whisking, but much weaker coupling during rest. However, several other studies, employing a variety of techniques, reported strong correlation between neuronal measurements (e.g., calcium or electrophysiological signals) and hemodynamic signals. For example, Mateo et al. reported intrinsic ultra-slow (0.1 Hz) fluctuations in arteriole diameter was entrained by the envelope of γ-band activity (Mateo et al., 2017). Such discrepancy can be potentially attribute to the following factors.

Firstly, the definition of the resting state is critical for examining the neural basis of the resting state BOLD signal. In animal studies, we can only rely on the external behaviors or stimulation to define the "resting state". Winder et al. employed detailed behavioral monitoring to specifically exclude all spontaneous behavior (e.g., volitional whisking) in head-fixed awake mice to establish the "resting state" periods. This step is especially important in the regions like somatosensory cortex, as the periods during volitional whisking or other body movements should be counted as the evoked state. The importance of those often overlooked small motor activity in the ongoing neural activity was emphasized in their recent review (Drew et al., 2018). In the current study the visual system was examined, and the it had little or no input inside the constantly dark scanner bore, thus ensuring a clean "resting state". Secondly, almost all previous studies examined the coupling relationship in the cortex, and the current study focused on the subcortical nuclei of SC and LGN. This could be an important difference, as SC and LGN differ from cortical regions from spontaneous neural activity to vasculature. Thirdly, different animal states (i.e., awake, sedated or anesthetized) might contribute to the variations of the results, as the animal state affects the spontaneous neural and vascular activities. Overall, the coupling of neural and hemodynamic signals in the resting states requires further examination to reach a consensus.

4.4. Technical limitations

The simultaneous calcium fiber photometry and fMRI approach, while being relatively convenient, has its own limitations. The calcium signal mainly reflects the spiking activity, which is one component of the overall neural activity. Previous studies have generally suggest the BOLD signal during the task was more correlated with LFP (indicator of synaptic activity) than MUA (multi-unit activity, indicator of spiking activity) (Logothetis et al., 2001; Logothetis and Wandell, 2004), as the synaptic activity is more energy consuming. This fundamental limitation of the calcium fiber photometry would limit our ability to examine the neurovascular coupling in both evoked and resting states. Ongoing development of various voltage sensitive indicators might overcome this limitation, but currently suffers from much lower SNR than calcium indicators like GCaMP6 (Kulkarni and Miller, 2017). Another limitation of the current study is no physiological parameters (e.g., respiration and cardiac signals) were recorded, thus future studies with additional physiological recording are needed to disentangle the complex relationship among physiological, neural and BOLD signals. Moreover, we have to assume some degree of spatial synchrony in the BOLD fMRI data for studying neurovascular coupling using the current fiber photometry approach, similar with most methods for recording neural activities, including electrophysiological recordings like LFP and MUA. In the

current analysis, time courses of 4 voxels immediately underneath the fiber tip were assumed to be related to the calcium signal. Additional limitation of the current study includes the use of anesthesia. The current anesthesia method, combined dexmedetomidine and low dose of isoflurane, was shown to preserve robust evoked BOLD signals and resting state functional connectivity (Brynildsen et al., 2017). However, anesthesia will inevitably affect some aspects of neural and vascular properties (Gao et al., 2017), and thus efforts need to be made to conduct similar research in awake animals in the future.

Acknowledgement

This work was supported by National Natural Science Foundation of China (Grant No. 81771821, No. 81801354), Hundreds of Talents Program of Chinese Academy of Sciences (to Z. L.), the Shanghai Municipal Science and Technology Major Project (Grant No. 2018SHZDZX05), the Strategic Priority Research Program of the Chinese Academy of Sciences (Grant No. XDB32030100). This work was also supported by National Natural Science Foundation of China (81871349, 61671228, and 61728107), Science and Technology Program of Guangdong (2018B030333001, and 2017B090912006), and a grant from Hong Kong Research Grant Council (RGC C7048-16G).

Appendix A. Supplementary data

Supplementary data to this article can be found online at https://doi.org/10.1016/j.neuroimage.2019.07.006.

References

Brynildsen, J.K., Hsu, L.M., Ross, T.J., Stein, E.A., Yang, Y., Lu, H., 2017. Physiological characterization of a robust survival rodent fMRI method. Magn. Reson. Imaging 35, 54–60.

Drew, P.J., Winder, A.T., Zhang, Q., 2018. Twitches, Blinks, and Fidgets: Important Generators of Ongoing Neural Activity. Neuroscientist, 1073858418805427.

Fox, M.D., Snyder, A.Z., Zacks, J.M., Raichle, M.E., 2006. Coherent spontaneous activity accounts for trial-to-trial variability in human evoked brain responses. Nat. Neurosci. 9, 23–25.

Fox, M.D., Zhang, D., Snyder, A.Z., Raichle, M.E., 2009. The global signal and observed anticorrelated resting state brain networks. J. Neurophysiol. 101, 3270–3283.

Gao, Y.R., Ma, Y., Zhang, Q., Winder, A.T., Liang, Z., Antinori, L., Drew, P.J., Zhang, N., 2017. Time to wake up: studying neurovascular coupling and brain-wide circuit function in the un-anesthetized animal. Neuroimage 153, 382–398.

Goense, J.B., Logothetis, N.K., 2008. Neurophysiology of the BOLD fMRI signal in awake monkeys. Curr. Biol. 18, 631–640.

Hansen, P.C., 2000. The L-curve and its use in the numerical treatment of inverse problems. In: Johnston, P. (Ed.), Advances in Computational Bioengineering. WIT Press.

Hillman, E.M., 2014. Coupling mechanism and significance of the BOLD signal: a status report. Annu. Rev. Neurosci. 37, 161–181.

Jaime, S., Gu, H., Sadacca, B.F., Stein, E.A., Cavazos, J.E., Yang, Y., Lu, H., 2017. Delta rhythm orchestrates the neural activity underlying the resting state BOLD signal via phase-amplitude coupling. Cereb. Cortex 1–15.

Kim, C.K., Yang, S.J., Pichamoorthy, N., Young, N.P., Kauvar, I., Jennings, J.H., Lerner, T.N., Berndt, A., Lee, S.Y., Ramakrishnan, C., Davidson, T.J., Inoue, M., Bito, H., Deisseroth, K., 2016. Simultaneous fast measurement of circuit dynamics at multiple sites across the mammalian brain. Nat. Methods 13, 325–328.

Kim, S.G., Ogawa, S., 2012. Biophysical and physiological origins of blood oxygenation level-dependent fMRI signals. J. Cereb. Blood Flow Metab. 32, 1188–1206.

Kulkarni, R.U., Miller, E.W., 2017. Voltage imaging: pitfalls and potential. Biochemistry 56, 5171–5177.

Liang, Z., Ma, Y., Watson, G.D.R., Zhang, N., 2017. Simultaneous GCaMP6-based fiber photometry and fMRI in rats. J. Neurosci. Methods 289, 31–38.

Logothetis, N.K., Pauls, J., Augath, M., Trinath, T., Oeltermann, A., 2001. Neurophysiological investigation of the basis of the fMRI signal. Nature 412, 150–157.

Logothetis, N.K., Wandell, B.A., 2004. Interpreting the BOLD signal. Annu. Rev. Physiol. 66, 735–769.

Lu, H., Wang, L., Rea, W.W., Brynildsen, J.K., Jaime, S., Zuo, Y., Stein, E.A., Yang, Y., 2016 Feb. Low- but not high-frequency LFP correlates with spontaneous BOLD fluctuations in rat whisker barrel cortex. Cereb. Cortex 26 (2), 683–694.

Lu, H., Zuo, Y., Gu, H., Waltz, J.A., Zhan, W., Scholl, C.A., Rea, W., Yang, Y., Stein, E.A., 2007. Synchronized delta oscillations correlate with the resting-state functional MRI signal. Proc. Natl. Acad. Sci. U. S. A. 104, 18265–18269.

Ma, Y., Shaik, M.A., Kozberg, M.G., Kim, S.H., Portes, J.P., Timerman, D., Hillman, E.M., 2016. Resting-state hemodynamics are spatiotemporally coupled to synchronized and symmetric neural activity in excitatory neurons. Proc. Natl. Acad. Sci. U. S. A. 113, E8463–E8471.

Magri, C., Schridde, U., Murayama, Y., Panzeri, S., Logothetis, N.K., 2012. The amplitude and timing of the BOLD signal reflects the relationship between local field potential power at different frequencies. J. Neurosci. 32, 1395–1407.

Mateo, C., Knutsen, P.M., Tsai, P.S., Shih, A.Y., Kleinfeld, D., 2017. Entrainment of arteriole vasomotor fluctuations by neural activity is a basis of blood-oxygenation-level-dependent "Resting-State" connectivity. Neuron 96, 936–948 e933.

Matsui, T., Murakami, T., Ohki, K., 2016. Transient neuronal coactivations embedded in globally propagating waves underlie resting-state functional connectivity. Proc. Natl. Acad. Sci. U. S. A. 113, 6556–6561.

Mitra, A., Kraft, A., Wright, P., Acland, B., Snyder, A.Z., Rosenthal, Z., Czerniewski, L., Bauer, A., Snyder, L., Culver, J., Lee, J.M., Raichle, M.E., 2018. Spontaneous infra-slow brain activity has unique spatiotemporal dynamics and laminar structure. Neuron 98, 297–305 e296.

Pan, W.J., Thompson, G.J., Magnuson, M.E., Jaeger, D., Keilholz, S., 2013. Infraslow LFP correlates to resting-state fMRI BOLD signals. Neuroimage 74, 288–297.

Pedregosa, F., Eickenberg, M., Ciuciu, P., Thirion, B., Gramfort, A., 2015. Data-driven HRF estimation for encoding and decoding models. Neuroimage 104, 209–220.

Rangaprakash, D., Wu, G.R., Marinazzo, D., Hu, X., Deshpande, G., 2018. Hemodynamic response function (HRF) variability confounds resting-state fMRI functional connectivity. Magn. Reson. Med. 80, 1697–1713.

Schlegel, F., Sych, Y., Schroeter, A., Stobart, J., Weber, B., Helmchen, F., Rudin, M., 2018. Fiber-optic implant for simultaneous fluorescence-based calcium recordings and BOLD fMRI in mice. Nat. Protoc. 13, 840–855.

Schmid, F., Wachsmuth, L., Schwalm, M., Prouvot, P.H., Jubal, E.R., Fois, C., Pramanik, G., Zimmer, C., Faber, C., Stroh, A., 2016. Assessing sensory versus optogenetic network activation by combining (o)fMRI with optical Ca2+ recordings. J. Cereb. Blood Flow Metab. 36, 1885–1900.

Scholvinck, M.L., Maier, A., Ye, F.Q., Duyn, J.H., Leopold, D.A., 2010. Neural basis of global resting-state fMRI activity. Proc. Natl. Acad. Sci. U. S. A. 107, 10238–10243.

Schulz, K., Sydekum, E., Krueppel, R., Engelbrecht, C.J., Schlegel, F., Schroter, A., Rudin, M., Helmchen, F., 2012. Simultaneous BOLD fMRI and fiber-optic calcium recording in rat neocortex. Nat. Methods 9, 597–602.

Schwalm, M., Schmid, F., Wachsmuth, L., Backhaus, H., Kronfeld, A., Aedo Jury, F., Prouvot, P.H., Fois, C., Albers, F., van Alst, T., Faber, C., Stroh, A., 2017. Cortex-wide BOLD fMRI activity reflects locally-recorded slow oscillation-associated calcium waves. Elife 6.

Shmuel, A., Leopold, D.A., 2008. Neuronal correlates of spontaneous fluctuations in fMRI signals in monkey visual cortex: implications for functional connectivity at rest. Hum. Brain Mapp. 29, 751–761.

Thompson, G.J., Merritt, M.D., Pan, W.J., Magnuson, M.E., Grooms, J.K., Jaeger, D., Keilholz, S.D., 2013. Neural correlates of time-varying functional connectivity in the rat. Neuroimage 83, 826–836.

Thompson, G.J., Pan, W.J., Billings, J.C., Grooms, J.K., Shakil, S., Jaeger, D., Keilholz, S.D., 2014a. Phase-amplitude coupling and infraslow (<1 Hz) frequencies in the rat brain: relationship to resting state fMRI. Front. Integr. Neurosci. 8, 41.

Thompson, G.J., Pan, W.J., Magnuson, M.E., Jaeger, D., Keilholz, S.D., 2014b. Quasi-periodic patterns (QPP): large-scale dynamics in resting state fMRI that correlate with local infraslow electrical activity. Neuroimage 84, 1018–1031.

Valdes-Hernandez, P.A., Sumiyoshi, A., Nonaka, H., Haga, R., Aubert-Vasquez, E., Ogawa, T., Iturria-Medina, Y., Riera, J.J., Kawashima, R., 2011. An in vivo MRI template set for morphometry, tissue segmentation, and fMRI localization in rats. Front. Neuroinf. 5, 26.

Wang, M., He, Y., Sejnowski, T.J., Yu, X., 2018. Brain-state dependent astrocytic Ca(2+) signals are coupled to both positive and negative BOLD-fMRI signals. Proc. Natl. Acad. Sci. U. S. A. 115, E1647–E1656.

Winder, A.T., Echagarruga, C., Zhang, Q., Drew, P.J., 2017. Weak correlations between hemodynamic signals and ongoing neural activity during the resting state. Nat. Neurosci. 20, 1761–1769.